Available online at www.sciencedirect.com
SCIENCE DIRECT®
Mechanics of Materials 35 (2003) 903–912
MECHANICS OF MATERIALS
www.elsevier.com/locate/mechmat

Brittle-to-ductile fracture transition in Fe–3wt.%Si single crystals by thermal crack arrest

Y. Qiao, A.S. Argon *

Department of Mechanical Engineering, Massachusetts Institute of Technology, 77 Massachusetts Avenue, Cambridge, MA 02139-4307, USA

Received 16 August 2002

Abstract

The brittle-to-ductile (BD) transition in fracture in Fe–3wt.%Si single crystals was studied through the arrest of cleavage cracks propagating up a temperature gradient under various loading rates. Through the dependence of the BD transition temperature on loading rate an activation energy for the overall fracture transition was determined to be $\Delta G^* = 0.096$ eV. This is very close to the measured activation energy of 0.1 eV for double kink nucleation on screw dislocations under high effective shear stresses in the range of 500 MPa in dilute solid solution iron alloys of Ni and Si and indicates that the BD transition by crack tip shielding was governed by the mobility of dislocations away from the crack tip. Observations of slip line patterns in the flank regions of the arrested cracks by Nomarski interference contrast microscopy provided direct verification of the expected modes of plastic crack tip shielding.

Keywords: Brittle-to-ductile fracture transition; Fe–3wt.%Si alloy

1. Introduction

Fracture transitions from brittle to ductile (BD), or vice versa, in intrinsically brittle metals, and particularly in Fe and steel continue to remain of considerable mechanistic interest. There have been numerous experimental and theoretical studies of the phenomenon in steel. An even partial accounting of the most recent work would be daunting and out of place in this short presentation. A brief accounting of the relevant experimental work was given recently by Argon (2001) and Gally and Argon (2001). Here we will be primarily interested in the experimental manifestation of the BD transition phenomenon in relation to possible mechanistic models, with particular emphasis on the elucidation of the key processes governing the transition.

While the transition from ductile to brittle (DB) is of greater technological interest in steels, the BD transition has lent itself to more precise experimentation, particularly in model materials such as Si (Gally and Argon, 2001, and references quoted therein) and some bcc metals (Hirsch and Roberts, 1996, and references quoted therein). A subject of greater interest than most has been the nature of the triggering mechanism that initiate ductile

* Corresponding author. Tel.: +1-617-253-2217; fax: +1-617-258-5802/8742.
E-mail address: argon@mit.edu (A.S. Argon).

0167-6636/03/$ - see front matter
doi:10.1016/S0167-6636(02)00293-4

response in the brittle cleavage regime. Recent models of the BD transition have considered key phenomena occurring at atomistically sharp crack tips. In the earliest developments by Rice and Thomson (1974) and more modern versions of it (Rice, 1992; Rice et al., 1992; Xu et al., 1995, 1997) the critical step is viewed to be the nucleation of an embryonic dislocation loop from the crack tip which then undergoes profuse multiplication to produce crack tip shielding. This form of response has been thought to be applicable to bcc metals where dislocation mobility is relatively unhindered by a very low level of resistance to kink motion along screw dislocations. In complementary considerations, the BD transition has been associated with sluggish mobility of dislocations away from crack tips as is the case in Si and possibly in most other covalent crystalline substances where the rate controlling process of crack tip shielding has been well established to be the mobility of dislocations away from the crack tip (see Argon, 2001 for an accounting of the experiments and models). Finally it has been proposed that the BD transition results from a collective process of autocatalytical multiplication of dislocation loops akin to models of defect mediated melting (Khantha et al., 1994, 2001; Khantha and Vitek, 1997).

In the recent experimental study of the BD transition in dislocation-free Si, Gally and Argon (2001) have probed the phenomenon by means of a thermal crack arrest experiment which for Si provided considerable insight into the nature of the transition. Here we report on the results of a similar experimental study in Fe–3wt.%Si single crystals.

2. Experimental details

2.1. Materials

The material consisted of a substantial size Fe–3wt.%Si single crystal originally extracted from a large ingot cast at Allegheny Ludlum Steel Co. [1] The composition in % by wt. consisted of 0.63C, 3.4Si, <0.01S and <0.01P. Long single crystal strips of dimensions $100 \times 10 \times 4$ mm were extracted from the large single crystal block by electrical discharge machining. The 100×4 mm surfaces of the strips were arranged to be parallel to the $\{0\,0\,1\}$ crystallographic planes, and the long dimensions were parallel to either the $\langle 1\,0\,0\rangle$ direction (group A) or parallel to the $\langle 1\,1\,0\rangle$ direction (group B). The strips were decarburized to lower the carbon content to <0.06% to eliminate carbides of often substantial size, but still permit dislocation decoration by carbon nanoprecipitates necessary for any possible etching technique. The stringent decarburization schedule is described in detail elsewhere (Qiao and Argon, 2003a). Since the deformation resistance of the alloy was governed substantially by the Si content which had not been changed, it remained unaltered. The level of the critical resolved shear stress (CRSS) and temperature dependence of the $\{1\,1\,0\}\langle 1\,1\,1\rangle$ slip system was determined from tension experiments and is reported elsewhere (Qiao and Argon, 2003a). The CRSS on this system at room temperature was close to 90 MPa.

The single crystal strips were electron beam (EB) welded into double cantilever beam (DCB) shaped carrier specimens according to a particular welding schedule to minimize residual stresses (for details see Qiao and Argon, 2003a). Upon EB welding, side grooves of 60° angle and 0.5 mm depth were machined into the DCB specimens along the median plane to constrain the cleavage path into the median plane, and a chevron of 45° was machined in front of the starter crack for effective initiation of cleavage fracture in the median plane. The final manufactured specimens were all given a mild annealing treatment at 400 °C for 2 h.

2.2. Experimental setup

The DCB specimens were pried apart by insertion of a hardened steel wedge with an angle of 10°, and surfaces lubricated with a graphite spray. The wedge was inserted at rates controlled by a hydraulic testing machine (Instron 1350). The far ends of the DCB specimens were surrounded by an induction heating coil powered by a type T-254-

[1] Provided to us in the late 1980s by Prof. F. Spaepen of Harvard.

225 Lepel induction heating power supply. The experiment was carried out inside a Centorr vacuum chamber under moderate vacuum to prevent oxidation of the specimens. This resulted in quite constant temperature gradients along the DCB specimens, with temperature ranging typically from 75–80 °C at the initial crack tips to about 150–170 °C at the far end where the cleavage cracks were to be arrested. Crack growth, which was always jerky, was not measured directly but was determined from compliance changes of the DCB specimens, monitored through the plot of the DCB specimen arm separation load P vs. arm separation displacement δ, according to standard beam theory relations.

2.3. Fractography and crack tip response determination

Fractography on the median plane of cleavage cracking was performed after the experiment was over, following the cryogenic breaking-apart of the DCB specimens. To assess crack tip plastic response associated with the thermal arrest of the cleavage crack both standard etching techniques (see Nadgornyi, 1988) as well as Berg–Barrett X-ray topographic imaging techniques (for a recent successful application of the technique see Gally and Argon, 2001) were tried but were on the whole unsuccessful in identifying the specific crystallographic aspects of the plastic response because of the quite rough nature of the cleavage surfaces.

Nomarski interference contrast microscopy of the crack tip region on the flanks of the cryogenically separated arms of the DCB samples proved to be much more successful.

3. Experimental results

Fig. 1 shows a typical response of the jerky advance of the cleavage crack along the median plane of the DCB specimens (A-100c), up the temperature gradient in the form of five discrete elastic jumps which eventually have put the crack tip into the high temperature region of thermal crack arrest that followed after some further load increase. This further load increase has not advanced the crack but initiated plastic shielding processes of the crack tip and began to plastically

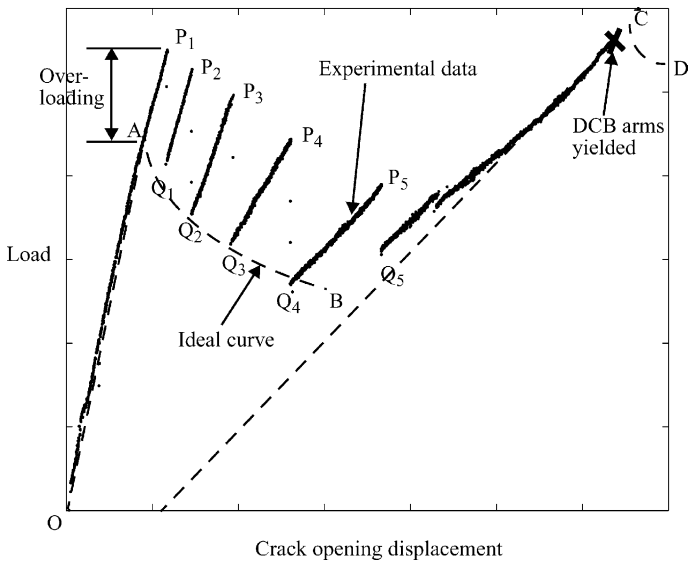

Fig. 1. A typical DCB specimen arm-separation-load vs. relative arm-opening-displacement plot (sample A-100c) for a cleavage crack made to propagate on the (0 0 1) plane parallel to the [1 0 0] direction, showing five intermediate jerky elastic brittle forms of advance before finally undergoing a thermal BD fracture transition upon further load increase between Q5 and C.

Table 1
Experimental results

Specimen number*	Group	Crack opening rate (mm/s)	T_{BD} (°C)	Temperature at cold end (°C)	Temperature at upper end (°C)	The number of crack jumps	Original crack length (mm)	Length of each crack jump (mm) K_{ICa} (MPa $\sqrt{m}$): K_{IC} for the crack to propagate K_{ICb} (MPa $\sqrt{m}$): K_{IC} at arrest the crack
100c	A	0.042	130	74	172	5	52.3	Jump length: 8.4; 10.2; 13.4; 16.4; 5.0 K_{ICa}: 7.6; 6.8; 8.2; 8.0; 9.1 ($\overline{K}_{ICa} = 7.9$) K_{ICb}: –; 5.4; 5.8; 5.7; 6.7; 7.6 ($\overline{K}_{ICb} = 6.2$)
100f	A	0.042	111	94	174	2	51.8	Jump length: 5.6; 4.1 K_{ICa}: 9.0; 7.8 ($\overline{K}_{ICa} = 8.4$) K_{ICb}: –; 7.2; 7.2 ($\overline{K}_{ICb} = 7.2$)
100g	A	0.0028	106	83	143	3	55.4	Jump length: 4.5; 7.0; 8.6 K_{ICa}: 7.8; 6.4; 8.3 ($\overline{K}_{ICa} = 7.5$) $\overline{K}_{ICb}$: –; 6.1; 7.4; 7.0 ($\overline{K}_{ICb} = 6.8$)
100h	A	0.0028	120	88	155	2	53.0	Jump length: 8.4; 18.1 $\overline{K}_{ICa}$: 7.1; 8.3 ($\overline{K}_{ICa} = 7.7$) $\overline{K}_{ICb}$: –; 7.2; 6.8 ($\overline{K}_{ICb} = 7.0$)
110e	B	0.040	124	97	177	2	53.7	Jump length: 13.6; 9.3 $\overline{K}_{ICa}$: 6.0; 7.5 ($\overline{K}_{ICa} = 6.8$) $\overline{K}_{ICb}$: –; 5.7; 6.4 ($\overline{K}_{ICb} = 6.1$)

* The thickness b and the height of DCB arm h of all the specimens are 4.0 and 19.0 mm, respectively.

bend the DCB specimen arms, indicative of a successful thermal arrest. The results of the four successful experiments of group A (cracks growing in the [1 0 0] direction) and a case of arrest in group B (crack growing in the [1 1 0] direction) are presented in Table 1. The table gives for each sample the DCB arm separation rate $\dot{\delta}$, the BD transition temperature, the several K_{ICa} values required to initiate crack jumps and the corresponding K_{ICb} values involved in each crack arrest, the lengths of the intermediate crack jumps, and the original crack lengths of the starter cracks are all presented. This permits determination of the final crack length at thermal arrest and the corresponding DCB total arm opening displacements. Considering that each K_{ICb} at crack arrest of the intermediate crack jumps are more reflective of the actual fracture toughness, an overall fracture toughness of $K_{\mathrm{IC}} = 6.66 \pm 0.17$ MPa $\sqrt{\mathrm{m}}$ was determined. The magnitude of this will be discussed later in Section 4.3.

Fig. 2 shows a representative SEM fractograph of the fracture plane after the final cryogenic separation of a DCB sample (A-100g) following thermal crack arrest. The fractograph shows the terminal region of the final crack jump of length 8.6 mm, from an initially smoothly curved form, (sketched in the figure, but not in its proper position) of the next-to-last jump position to the more highly curved final arrest front. The curved nature of the crack front between side grooves during the advance of the crack, prior to the final thermal arrest site, is consistent with the so-called *vertex* nature of the stress intensity at the surface in cases of purely elastic crack advance (see Riedel, 1987), where a different and much lower form of singularity is thought to prevail. The actual shapes of the intermediate crack front positions could be traced as curves normal to the local field of cleavage river markings. There was no evidence of any crack blunting effect at any of the several intermediate elastic crack arrest sites, which were mostly difficult to discern and could only be identified from occasional sites of reinitiation of new cleavage river-marking fans.

A goal of the experiments was to develop some insight into the crystallographic nature of the thermally assisted plastic response during the final BD transition. To develop such insight into the governing rate process, $1/T_{\mathrm{BD}}$ was plotted against the natural log of a normalized measure of the reciprocal waiting time at the last crack arrest site for the development of successful plastic crack tip shielding, or blunting, events that render the crack immobile. The parameter that was chosen for this process is

$$v = \left(\frac{\dot{\delta}}{\delta}\right)\left(\frac{L_{\mathrm{f}}^2}{hc}\right) = \left(\frac{\dot{K}_{\mathrm{I}}}{K_{\mathrm{ICb}}}\right) \Big/ v_{\mathrm{f}} \tag{1}$$

where L_{f} is the final crack length (final DCB arm length) at the last arrest site; h, the DCB arm

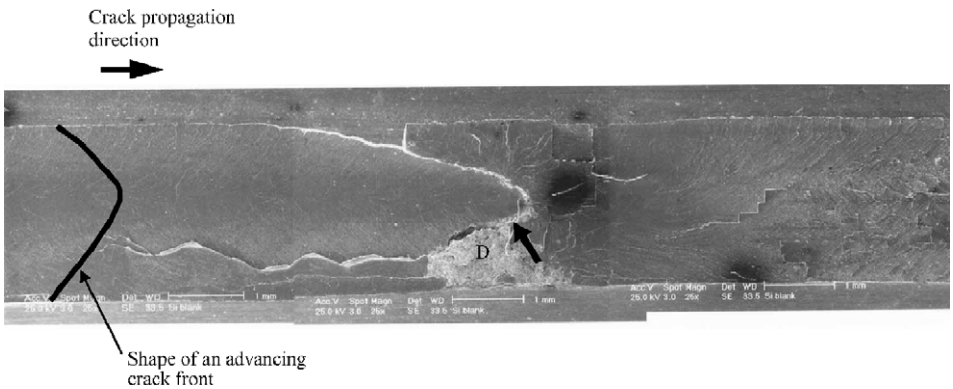

Fig. 2. A montage of SEM fractographs of the final arrest site in sample A-100g. The curved contour shows a typical shape of an advancing cleavage crack front. The region designated with D shows ductile dimple fracture that is thought to have resulted in the further loading after the thermal arrest processes of plastic relaxations have occurred at the crack tip.

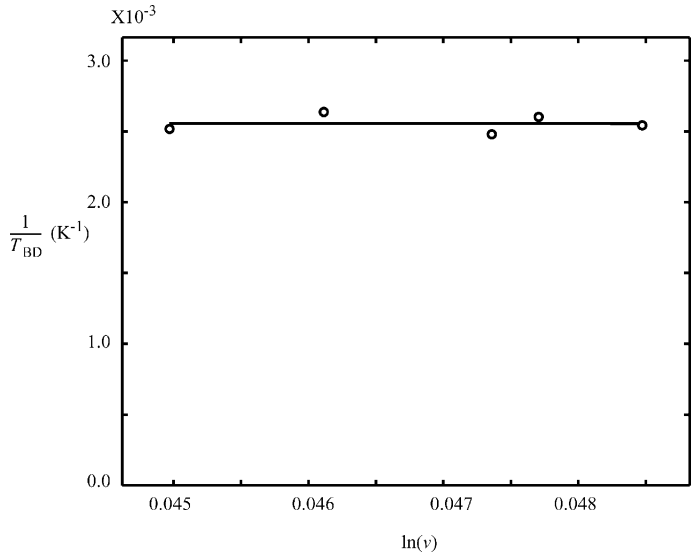

Fig. 3. Dependence of the BD transition temperature on the loading rate in the final stage of crack tip response. The slight slope indicates an activation energy of 0.096 eV.

height; c, the longitudinal velocity of sound of Fe; and v_f, the bending vibration frequency of the final DCB arm.

The plot is shown in Fig. 3. It gives a very small activation energy of $\Delta G^* = 0.096$ eV.

4. Discussion

4.1. Character of possible slip activity at thermal arrest site

Fig. 4a and b shows the possible crystallographic slip systems of the $\{1\,1\,0\}\langle 1\,1\,1\rangle$ type at the tips of the cracks propagating in the $\langle 1\,0\,0\rangle$ direction (group A) and in the $\langle 1\,1\,0\rangle$ direction (group B), respectively, sketched on reference cubes. In each case three different possible slip systems were identified. As indicated in the figure, for group A they are labelled as: the inclined planes (ia), the oblique planes (oa), and the rotated vertical planes (rva); for group B they are labelled as: the obliques planes (ob), the inclined planes (ib), and the vertical planes (vb), respectively. The forms of slip traces due to these systems that should be observed on the $\{0\,0\,1\}$ cleavage surface are sketched below the reference cubes of Fig. 4a and b. To assess the level of activity on these planes the distribution of the resolved shear stresses on them in the directions of the appropriate Burgers vectors were calculated from the anisotropic crack tip solution of Hoenig (1982) which gives the resolved shear stresses, τ_{nm} (n normal to the slip plane; m parallel to the relevant slip direction), on these planes as:

$$\tau_{nm} = \frac{K_{\text{appl}}}{\sqrt{2\pi\rho}} g_{nm}(\tilde{\varphi}, \tilde{\psi}) \tag{2}$$

where K_{appl} is the applied mode I stress intensity; ρ, the radial distance on the slip plane, from the crack tip; $\tilde{\varphi}$, the angle between the line of intersection between the slip plane and the $\{0\,0\,1\}$ cleavage plane and the radial direction given by ρ; and $\tilde{\psi}$, the angle between the slip plane and the $\{0\,0\,1\}$ cleavage plane. The details of the developments that lead to Eq. (2) can be found elsewhere (Gally and Argon, 2001; Qiao, 2002). The distributions of the calculated absolute values of the resolved shear stresses in the various slip planes are given as functions of the specific angles $\tilde{\varphi}$ of the individual systems in Fig. 5a and b, for the group A experiments and the group B experiment, respectively. Examination of the figures shows that the maximum resolved shear stresses, as represented by the factor $g_{nm}(\tilde{\varphi}, \tilde{\psi})$, range for group A

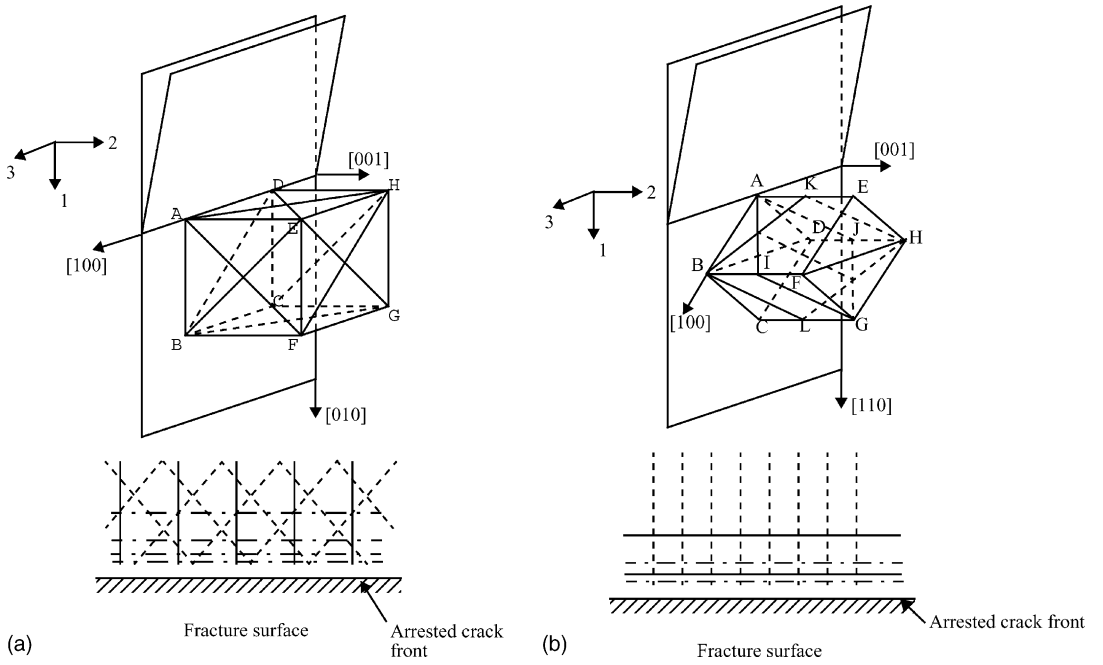

Fig. 4. (a) Unit bcc cube showing the possible activable slip systems at the arrested crack tip for a crack propagating parallel to the [1 0 0] direction: oblique planes/slip directions (ABGH/AG,HB; DEFC/DF, EC) designated as "oa" (solid lines); rotated vertical planes/slip directions (DHFB/DF, HB; AEGC/AG, EC) designated as "rva" (dashed lines); inclined planes/slip directions (EHCB/HB, EC; ADGF/DF, AG) designated as "ia" (dashed-dotted lines). The sketch below shows expected slip traces on cleavage plane flanks. (b) Unit bcc cube showing the possible activable slip systems at the arrested crack tip for a crack propagating parallel to the [1 1 0] direction: inclined planes/slip directions (AJGI/AG;EICJ/EC) designated as "ib" (solid lines); oblique planes/slip directions (BKHL/BH; FKDL/DF) designated as "ob" (dashed lines); vertical planes/slip directions (BDHF/BH, DF) designated as "vb" (dashed-dotted lines). The sketch below shows expected slip traces on cleavage plane flanks.

samples in the descending order as: 0.343, 0.318, and 0.213, for the oblique planes (oa), the rotated vertical planes (rva), and inclined planes (ia), respectively. For the group B sample they range as: 0.322, 0.271, and 0.198, for the inclined planes (ib), the oblique planes (ob), and the vertical planes (vb), respectively. If no other considerations were to apply, the level of activity on these planes might be expected to be paralleling these orders of resolved shear stresses.

As mentioned already above, the etch pitting technique and the Berg–Barrett X-ray topographic imaging techniques to outline actual slip systems were indecisive and gave very disappointing results. Examination of the crack flanks in the thermal arrest front by Nomarski interference contrast microscopy, however, proved much more fruitful. Fig. 6a–c shows such light optical micrographs for sample A-100g on the crack flank close to the arrested crack tip in the region shown with the arrow in Fig. 2. They show the outlines of the rotated vertical planes (rva) near the crack front (Fig. 6a); the oblique planes (oa) (Fig. 6b) and the inclined planes (ia) (Fig. 6c) somewhat farther back, indicating that all these slip systems have indeed been active with the traces of the last two systems showing up a fraction of a mm behind the crack tip region of high curvature. Since the crack front shape was quite curved the actual stress levels and their ordering must have been considerably different from the predictions for a straight crack front. The nature of the slip traces and their locations indicated that the final crack jump of 8.6 mm for this crystal, to the eventual curved contour occurred in a purely elastic and brittle manner. The crack tip plasticity through the activation of the various slip systems to result in the crack tip shielding, and possibly blunting, then occurred

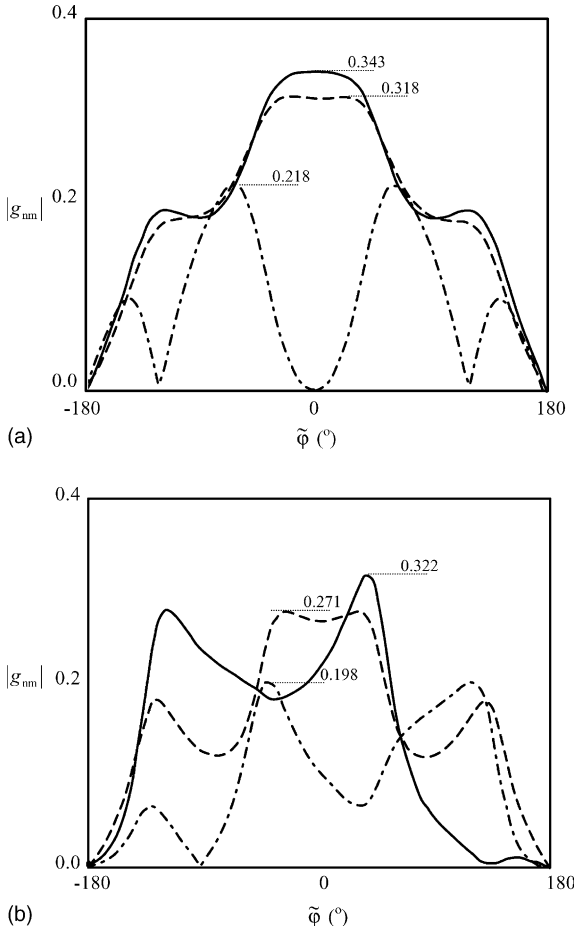

Fig. 5. (a) The angular distributions of calculated coefficients g_{nm} of the CRSS: on the oblique planes (solid line); on the rotated vertical planes (dashed line); on the inclined planes (dashed-dotted line) for a crack advancing parallel to the [1 0 0] direction; (b) the distributions of calculated coefficients g_{nm} of the CRSS: on the inclined planes (solid line); on the oblique planes (dashed line); on the vertical planes (dashed-dotted line) for a crack advancing parallel to the [1 1 0] direction.

subsequently during the continued load increases when the crack remained stationary, along the path Q5 to C for the corresponding case of the loading history of sample A-100c shown in Fig. 1.

4.2. Crack arrest as a rate process

In our earlier bi-crystal fracture experiments (Qiao and Argon, 2003a) and cleavage cracking experiments through polycrystals (Qiao and Argon, 2003b) in Fe–3wt.%Si and Fe–2wt.%Si alloy respectively, at low temperature, in the −20 °C range, no substantial evidence was found of plasticity outside some minor bending of and rubbing-together of cleavage ligaments and ledges. Under these conditions, particularly in Fe, even in the solid solution strengthened form, little resistance should be expected to kink motion along screw dislocations, making the dislocation mobility controlled primarily by kink pair nucleation (Sěstak and Seeger, 1978a,b). Then, if dislocations are initially locked, or are initially too few to initiate plastic response, the BD transition might be expected to be governed by dislocation emission from crack tips as considered by Xu et al. (1997). On the other hand while such emission of dislocations from crack tips may very often be a necessary condition, as recently demonstrated in Si by Gally and Argon (2001) and Argon and Gally (2001), the actual final BD transition may still be controlled by the mobility of the generated dislocations away from the crack tip, as has been advocated by Hirsch and Roberts (1996, with references cited therein) for several bcc metals. In the latter case the rate controlling process is expected to be the nucleation of double kinks along screw dislocations. On that basis our determination of the activation energy associated with the BD transition as 0.096 eV becomes quite relevant and is in good support of the latter hypothesis of mobility control. This is based on the study of Chen et al. (1981) of the rate controlling processes of plastic deformation in solid solution modified Fe, with Ni and Si in solution, where the stress dependence of the activation energy of double kind nucleation was determined experimentally. It was found there that regardless of solute content, at high stress levels where the double kink spacing becomes very close the activation energy decreases to a level of roughly 0.1 eV for effective shear stress levels in the range of 500 MPa and above. These effective shear stress levels are expected to be prevalent in the stalled crack tip arrest sites in our experiments, making our measured activation energy indicate that the BD transition in our experiments was also, most likely, governed by the mobility of dislocations accomplishing the eventual crack tip shielding.

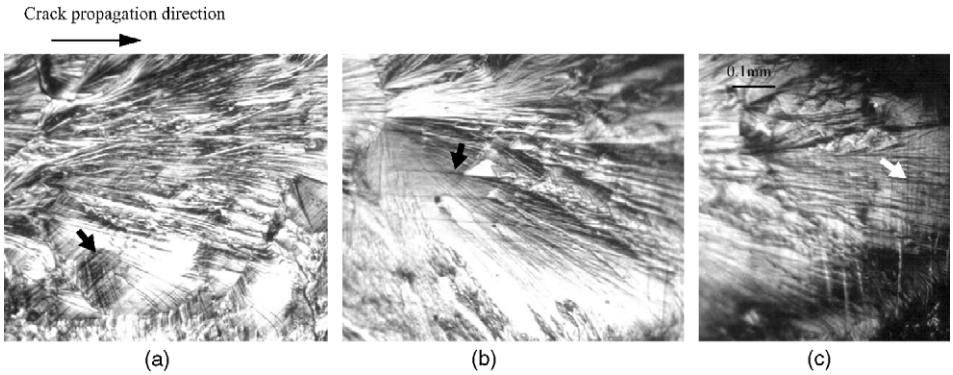

Fig. 6. Observed slip lines on the flanks of the cleavage fracture surface of sample A-100g, as viewed by Nomarski interference contrast microscopy in the area designated with the arrow in Fig. 2: (a) rotated vertical slip system; (b) oblique slip system; and (c) inclined slip system.

4.3. Level of measured fracture toughness

The measured average level of fracture toughness obtained from the multiplicity of elastic crack arrest processes, at the level of 6.66 MPa $\sqrt{\text{m}}$, which corresponds to a specific work of fracture (critical energy release rate) of $G_{IC} \approx 160$ J/m^2, is much larger than the measured values obtained by Gilman (1960) on Fe ($K_{IC} = 2.4$ MPa $\sqrt{\text{m}}$; $G_{IC} = 20.97$ J/m^2). Thus, the results of our experiments give an increase of 2.78 for the K_{IC} and 7.63 for G_{IC}.

In our recent experiments on the fracture resistance of individual grain boundaries in bi-crystal samples, these differences were even larger with a factor of 5.87 for K_{IC} and 40.5 for G_{IC} (Qiao and Argon, 2003a). In that study the difference was explained by a *process zone model* based on the analysis of Andersson and Bergkvist (1970) where the high work of separation was attributed to the substantial relative plastic shearing work of separation to connect the adjacent cleavage fracture strips. The latter having developed at different elevations relative to the median fracture plane when the cleavage process is shunted to different parallel levels as it went through a dense field of pre-existing deformation twins, producing an rms fracture surface roughness of 2.7 μm. The same effect was found in our present experiments where twins were not present but a very rough cleavage fracture surface of rms roughness of 1.8 μm developed nevertheless.

4.4. General observations

BD transition experiments in recent times in Si and in some bcc metals have been most widely carried out by performing fracture initiation experiments in cracked samples at different temperatures and different loading rates (see Argon, 2001). In these experiments the rate of increase in driving forces ($\dot{K}_I$) competes against crack tip shielding due to rate dependent plastic relaxation at the crack tips. Brittle behavior results when the driving forces increase at rates faster than the competing shielding rates. Under conditions of higher temperature and lower levels of $\dot{K}_I$ full shielding develops prior to reaching conditions of brittle crack propagation (Argon et al., 1996; Argon, 2001). In this form of experimentation the same crack tip elements undergo complex histories of stress increase and stress relaxation. In contrast to these experiments we have advocated crack arrest experiments in which cracks propagating at various constant velocities in a temperature gradient demonstrate a transition from brittle cleavage to tough behavior when the residence time of high crack tip stress in a material element become larger than the characteristic time for full stress relaxation (Brede et al., 1991; Gally and Argon, 2001). While the scenario of this experiment is appealing, operationally achieving the desired condition of propagating brittle cracks controllably at different velocities have proved to be exceedingly difficult because of the extreme sensitivity of

brittle cracks to small perturbations. Thus, in practice when brittle cracks advance only in a jerky manner the crack tip conditions during each arrest, leading to the final one become identical to the static experiments.

5. Conclusions

In experiments of BD transition by crack arrest under different loading rates up a temperature gradient in single crystals of Fe–3wt.%Si, jerkily advancing cracks were eventually arrested by thermal processes of plastic crack tip shielding. The measured activation energy for the BD transition was found to be close to 0.1 eV, which is in very good agreement with activation energies of double kink nucleation along screw dislocations that is known to control their mobility. Clear evidence was found for the expected crack-tip slip systems that were expected for the geometries of crack advance.

Acknowledgement

This research was supported by the National Science Foundation under Grant DMR-9906613.

References

Andersson, H., Bergkvist, H., 1970. J. Mech. Phys. Solids 18, 1.
Argon, A.S., 2001. J. Eng. Mater. Tech. 123, 1.
Argon, A.S., Gally, B.J., 2001. Scripta Mater. 45, 1287.
Argon, A.S., Xu, G., Ortiz, M., 1996. In: Chan, K.S. (Ed.), Cleavage Fracture: George R. Irwin Symposium. TMS, Warrendale, PA, p. 125.
Brede, M., Hsia, K.J., Argon, A.S., 1991. J. Appl. Phys. 70, 758.
Chen, Y.T., Atteridge, D.G., Gerberich, W.W., 1981. Acta Metall. 29, 1171.
Gally, B.J., Argon, A.S., 2001. Phil. Mag. 81, 699.
Gilman, J.J., 1960. J. Appl. Phys. 31, 2208.
Hirsch, P.B., Roberts, S.G., 1996. In: Chan, K.S. (Ed.), Cleavage Fracture: George R. Irwin Symposium. TMS, Warrendale, PA, p. 137.
Hoenig, A., 1982. Eng. Fract. Mech. 16, 393.
Khantha, M., Vitek, V., 1997. Acta Mater. 45, 4675.
Khantha, M., Pope, D.P., Vitek, V., 1994. Phys. Rev. Lett. 73, 684.
Khantha, M., Vitek, V., Pope, D.P., 2001. Mater. Sci. Eng. 319–321, 484.
Nadgornyi, N., 1988. In: Christian, J. et al. (Eds.), Dislocation dynamics and mechanical properties of crystals. In: Progress in Materials Science, vol. 31. Pergamon Press, Oxford.
Qiao, Y., 2002. Role of grain boundaries in cleavage cracking and thermal crack arrest experiments in iron–silicon alloy. Ph.D. thesis. The Department of Mechanical Engineering, MIT, Cambridge, MA.
Qiao, Y., Argon, A.S., 2003a. Mech. Mater., in press. PII: S0167-6636(02)00284-3.
Qiao, Y., Argon, A.S., 2003b. Mech. Mater. 35, 129–154.
Rice, J.R., 1992. J. Mech. Phys. Solids 40, 239.
Rice, J.R., Thomson, R., 1974. Phil. Mag. 29, 73.
Rice, J.R., Beltz, G.E., Sun, Y., 1992. In: Argon, A.S. (Ed.), Topics in Fracture and Fatigue. Springer, NY, p. 1.
Riedel, H., 1987. Fracture at High Temperatures. Springer, Berlin, p. 290.
Sëstak, B., Seeger, A., 1978a. Z. Metall. 69, 195.
Sëstak, B., Seeger, A., 1978b. Z. Metall. 69, 355.
Xu, G., Argon, A.S., Ortiz, M., 1995. Phil. Mag. 72, 415.
Xu, G., Argon, A.S., Ortiz, M., 1997. Phil. Mag. 75, 341.